Dynamic Compaction of Titanium Aluminides by Explosively Generated Shock Waves: Microstructure and Mechanical Properties

A. FERREIRA, M.A. MEYERS, and N.N. THADHANI

A detailed microstructural analysis and evaluation of the mechanical properties of titanium aluminides consolidated by novel shock processes[13] are presented. Successful consolidation was obtained and was evidenced by strong bonding between individual particles. Additions of Nb and Ti and Al elemental powders resulted in enhanced interparticle bonding through intense plastic deformation of Nb and shock-induced reactions between Ti and Al. Rapid cooling of interparticle molten layers yielded amorphous Ti-Al alloys; this interparticle melting and rapid cooling are a unique feature of shock processing. Embrittlement of individual particles of Ti_3Al-based alloy after exposure to 550 °C and 750 °C was observed. There is evidence of phase transformation after preheating the powder, and this fact can explain the high density of cracks obtained with this alloy after high-temperature shock consolidation. Mechanical properties of the Ti_3Al-based alloy were determined at room temperature and the fracture modes were studied. The microstructural observations are correlated with the mechanical properties.

I. INTRODUCTION

THE 1980s witnessed a great interest in intermetallic compounds, particularly in nickel and titanium aluminides. The increased interest is due to the desire to reduce the weight and improve the performance of aircraft turbine engines. The alloys based on titanium aluminides are emerging as attractive candidates because of their interesting properties: good strength at ambient temperature and good strength and high stiffness retention at high temperatures. More specifically, TiAl has a higher modulus at 1000 °C and Ti_3Al has a higher modulus at 815 °C than Ti at room temperature,[1,2] and the strength of TiAl does not drop with temperature until approximately 600 °C.[3] Titanium aluminides also present good oxidation resistance because of the protective oxide coating provided by aluminum. However, a generic problem with titanium aluminides is their low ductility and poor fracture toughness at room temperature,[2–6] making them difficult to fabricate.

The most successful method of improving the ductility of Ti_3Al has been the addition of β-stabilizing elements,[7] such as Nb. Niobium additions increase the nonbasal slip activity[2,7,8] and also result in microstructural refinement,[7,8] which has the effect of reducing the slip length. Furthermore, if enough Nb is added, a two-phase microstructure is retained ($\alpha_2 + \beta$),[6] in which the presence of a more ductile body-centered cubic (bcc) phase (β) helps to increase the ductility. Another method for increasing the ductility is to introduce a second phase, by rapid solidification, in order to homogenize the planar slip.[9,10,11] However, the rapidly solidified particles must be consolidated by a convenient process so that the properties acquired by rapid solidification are not lost due to the long thermal excursions in conventional powder processing techniques. Shock compaction is an attractive process for these materials, because the surfaces of the particles melt and rapidly resolidify while the particle interiors undergo only moderate heating.

The objectives of this article are to present the microstructural features and mechanical properties resulting from dynamic compaction of rapidly solidified titanium aluminides by explosively generated shock waves.

II. EXPERIMENTAL PROCEDURE

The shock consolidation of the rapid solidification processed (RSP) Ti-aluminide powders were conducted using double-cylinder tube implosion geometry.[12] The detailed description of the experimental setup, as-received powder characteristics, and the macroscopic features of the compacts are presented by Ferreira *et al.*[13] The microstructure and morphology of the starting powders were characterized by optical and scanning electron microscopy (SEM). Since some of the experiments were performed at high temperatures, the stability of the powders was also characterized after exposure at 550 °C and 750 °C. The titanium aluminide powders were sealed in evacuated quartz tubes and heated at the desired temperatures for 30 minutes, cooled to room temperature, and examined by optical, scanning electron microscopy, and X-ray diffraction.

For optical and SEM, the alloy powders and compacted specimens were mounted in lucite, metallographically polished, and etched using Kroll's reagent. For transmission electron microscopy, thin slices cut from the bulk compacts were electropolished in a solution consisting of 60 vol pct methanol, 37 vol pct butyl cellosolve, and 3 vol pct perchloric acid at a −40 °C and 25 to 30 V range. Transmission electron microscopy (TEM)

A. FERREIRA, Professor and Lieutenant Colonel, is with the Military Institute of Engineering, Urca, Rio de Janeiro, RJ 22093, Brazil. M.A. MEYERS, Professor, is with the Department of Applied Mechanics and Engineering Sciences, University of California–San Diego, La Jolla, CA 92093-0411. N.N. THADHANI, Associate Research Professor, is with the Center for Explosives Technology Research, New Mexico Institute of Mining and Technology, Socorro, NM 87801.

Manuscript submitted September 5, 1989.

was performed with a PHILIPS* CM 30 microscope at an accelerating voltage of 200 keV.

*PHILIPS is a trademark of Philips Electronic Instruments Corporation, Mahwah, NJ.

The basic compositions of the as-received titanium aluminide powders are: Ti-21 wt pct Nb-14 wt pct Al (designated Ti_3Al) and Ti-30.9 wt pct Al-14.2 wt pct Nb (designated TiAl). The chemical compositions of these two alloys are given in Table I of Ferreira *et al.*[13] Approximately 1 wt pct erbium was present in these alloys to create a dispersion of erbium oxide. Additionally, these alloys contained different amounts of carbon varying from 0.015 wt pct for Ti_3Al to 0.5 wt pct for TiAl alloys (reported in Table I of Ferreira *et al.*[13]).

Mechanical tests were performed at ambient temperature in an MTS 810 or INSTRON 1122 testing machine. For specimens exhibiting large density of cracks, compression and flexure tests were carried out, whereas for specimens with fewer cracks, tensile tests were performed. Compression tests were done using cylindrical specimens with a diameter of 6 mm and a height of 12 mm. Special compression plates using a disc of tungsten carbide in the center were used in order to prevent plastic deformation of the plates during the test. An extensometer attached to the compression plates enabled specimen deformation to be measured and recorded accurately. Uniaxial tension specimens were cut from transverse cross sections (30-mm long, 10-mm wide, and 1.5-mm thick), and samples with 7-mm gage length and 4-mm width were prepared by hand filing after being sandwiched between two templates. The specimens were fastened in holders that could slide in a special guide in order to permit alignment with the grips of the testing machine and to eliminate bending stresses. Four-point bend tests were performed on 4-mm by 4-mm by 30-mm long specimens. The flexural strength was considered to be the maximum outer fiber stress at time of failure, regardless of where fracture originated in the load span.

All specimens were electrolytically polished prior to testing and the constant crosshead speed was calculated in order to produce an engineering strain rate of 10^{-4} s^{-1} in all cases. Representative samples of specimens that failed in mechanical tests were selected for fractographic studies in a Hitachi Perkin Elmer model HHS-2R scanning electron microscope.

III. RESULTS AND DISCUSSION

Prior to discussing the properties of the shock-compacted titanium aluminides, the microstructural characteristics of the as-received RSP alloy powders will

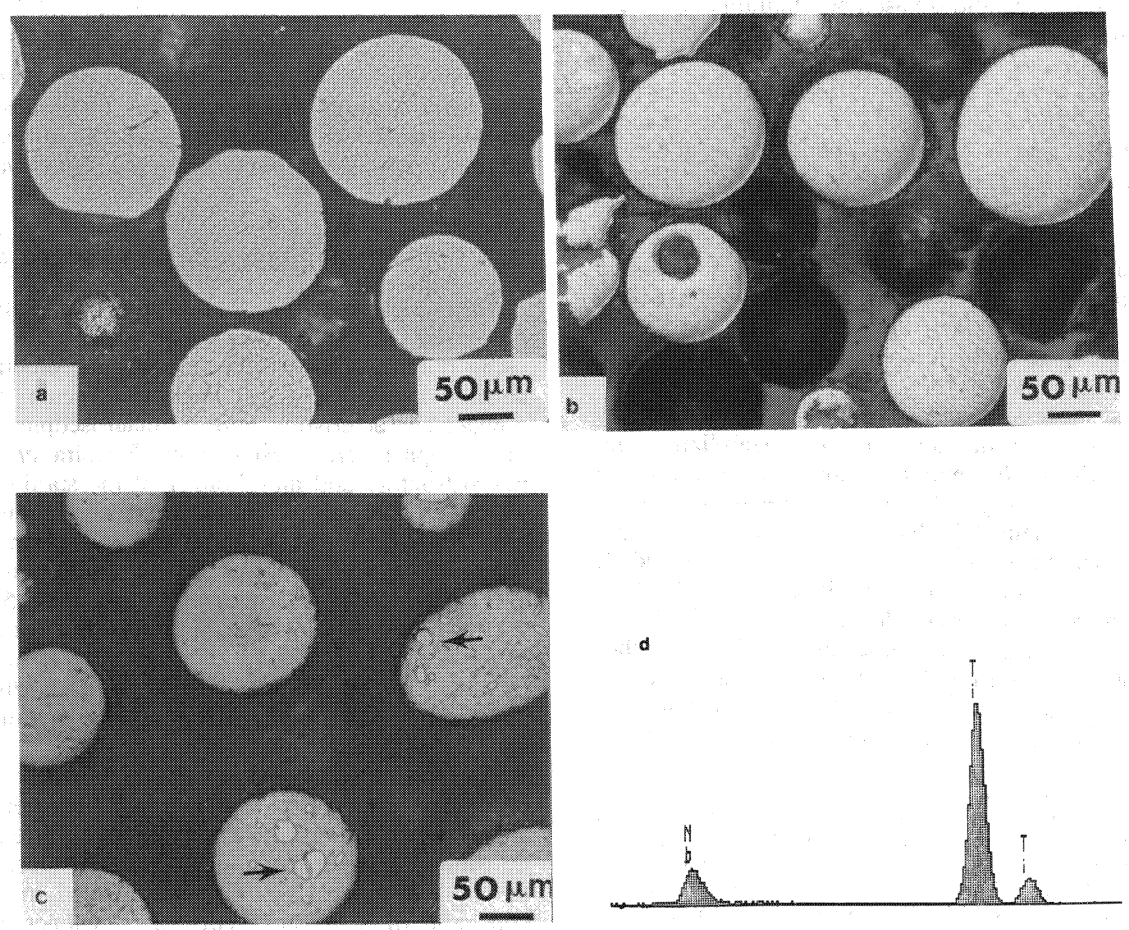

Fig. 1—Optical micrographs of powder particles of (*a*) Ti_3Al-based alloy and (*b*) TiAl-based alloy. (*c*) Optical micrograph of powder particles of TiAl-based alloy and (*d*) EDX analysis from bright points inside particles.

be presented (Section III–A). The microstructure of the shock-consolidated materials, as determined by optical and SEM, will be presented in Section III–B, followed by detailed TEM characterization of the substructure in particle interiors and grain boundaries (Section III–C). Finally, the mechanical properties and their correlation with microstructure will be discussed in Section III–D.

A. *Microstructural Characteristics of As-Received Powder Material*

The Ti_3Al and TiAl alloy powders in general possessed a mixture of microcellular and polycrystalline structure. Optical micrographs (Figures 1(a) through (d)) show the typical morphology and structure of the Ti_3Al and TiAl powders. Some of the powder particles had an internal void (Figure 1(b)), possibly caused by gas entrapment during the rapid solidification. Some other powders also had Nb incorporated into the chemical composition (Figures 1(c) and (d)).

Exposure of the Ti_3Al + Nb alloy powder to a temperature of 550 °C for 1 hour resulted in the generation cracks within the particles, as shown in Figure 2(a). Scanning electron microscopy and energy dispersive X-ray (EDX) analysis (Figure 2(b)) showed fine round white-contrast Er_2O_3 precipitates uniformly decorating the cell (or grain) boundaries. Evidence of phase transformations in the Ti_3Al alloy powder after heat treatment at 550 °C was also obtained by X-ray diffraction (Figure 3). As the temperature is raised up to 750 °C, the metastable β phase (bcc) starts to decompose into the more stable α_2 phase (hexagonal close-packed, hcp) (with lattice parameters a = 0.578 nm and c = 0.466 nm[14]) and also into an orthorhombic phase (with a = 0.450 nm, b = 0.588 nm, and c = 0.960 nm). Such phase transformations have also been reported by Banerjee *et al.*,[14] Strychor *et al.*,[15] and Kaufman *et al.*[16] The present results confirm Strychor *et al.*'s[15] and Kaufman *et al.*'s[16] observations and indicate that this alloy composition has severe temperature limitations.

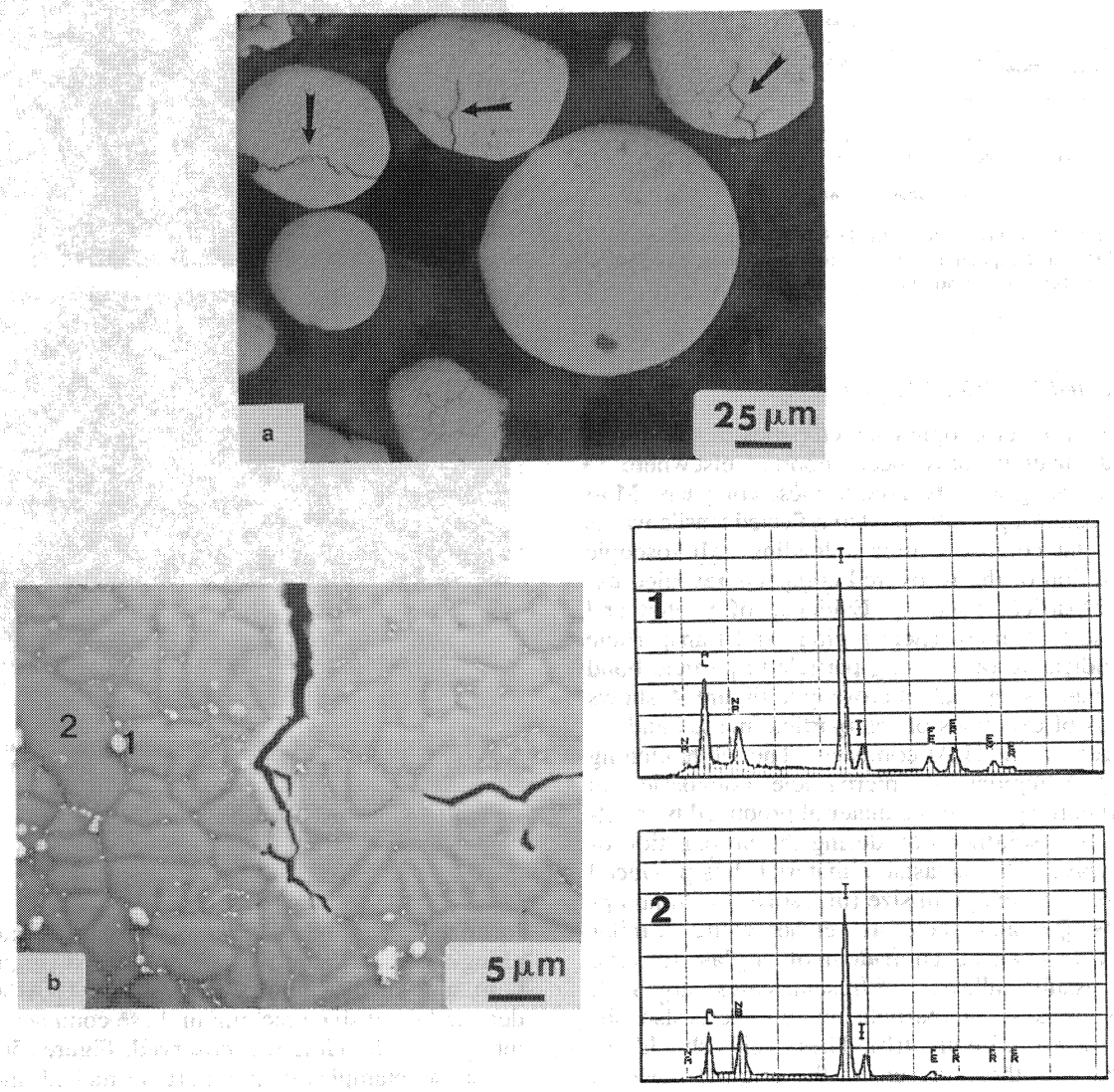

Fig. 2—(*a*) Optical micrograph of Ti_3Al + Nb powder, showing cracks generated after heat treatment at 550 °C. (*b*) Scanning electron micrograph of the Ti_3Al particle after exposure at 550 °C and EDX analysis from region (1) showing round Er_2O_3 precipitate and from region (2) containing matrix material.

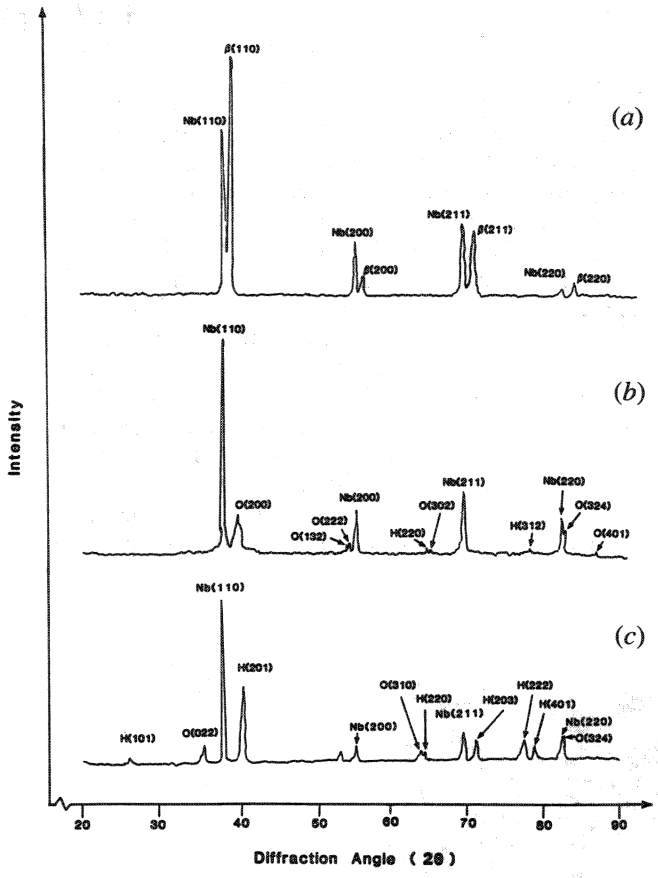

Fig. 3—X-ray diffraction pattern of Ti_3Al + Nb powder after exposure at different temperatures: (*a*) room temperature, (*b*) 550 °C, and (*c*) 750 °C (O = orthorhombic; H = hexagonal).

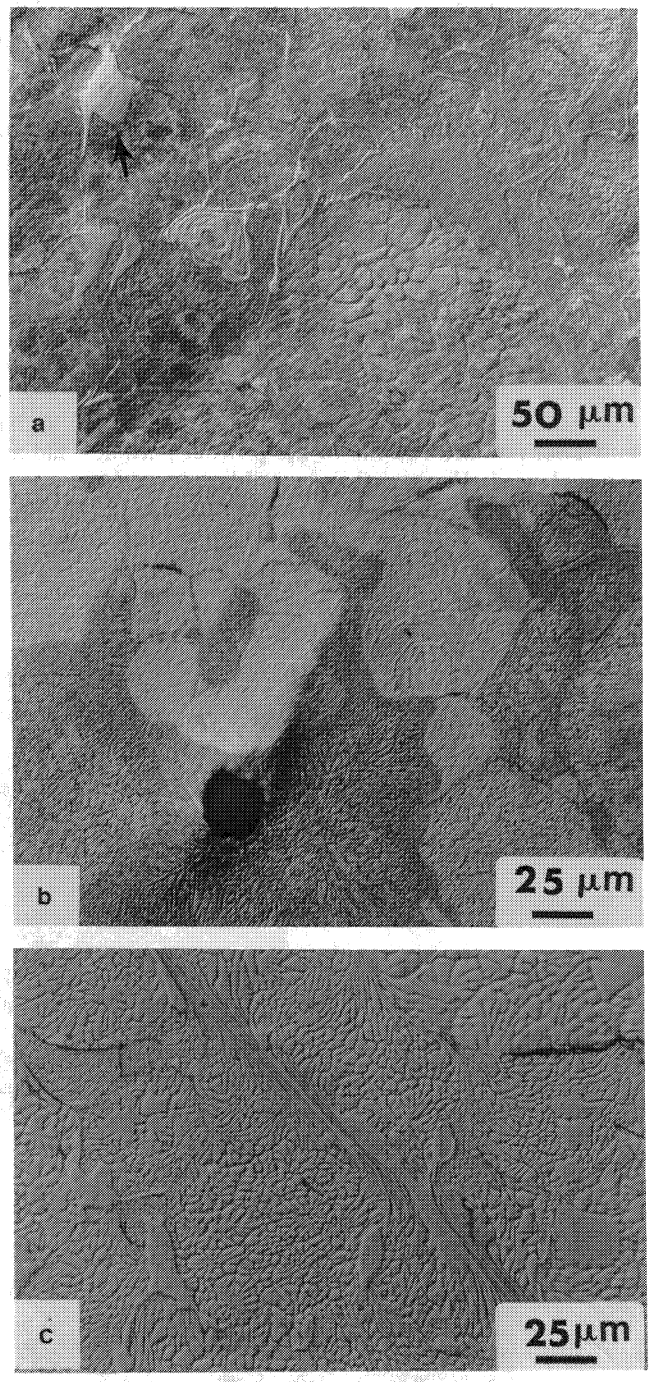

Fig. 4—Micrographs of typical interparticle regions in Ti_3Al alloys showing (*a*) evidence of melted and rapidly solidified material and (*b*) shrinkage void at the center of the melting pool. (*c*) Localized shear deformation and interparticle melting.

B. *Compacted Material Characteristics*

The general macroscopic characteristics of the shock-compacted materials have been reported elsewhere.[13] Extensive cracking was observed in these compacts. Most of the macrocracking is attributed to reflected tensile waves formed in the compacts after unloading. Microscopic characterization of the recovered compacts revealed excellent interparticle bonding. Evidence of melted and rapidly solidified interparticle regions and transparticle cracking indicative of a strong particle-to-particle bond were obtained by optical microscopy. Figure 4 shows micrographs of examples of interparticle melted and resolidified regions in Ti_3Al compacts. The white etching (contrast-free) regions at interparticle boundaries in Figure 4(a) correspond to the material produced by melting and rapid resolidification during the propagation of the shock wave. The metastable material thus produced has an extremely fine grain size (unresolved with an optical microscope) and, therefore, etches white. Similar observations have also been made in other glass-forming and microcrystalline alloys.[17–20] In some cases, large melt pools with voids at interparticle regions were also observed, as shown in Figure 4(b). These voids should not be confused with those present in the original powders (Figure 1(b)) but were formed at interparticle melt regions during the consolidation process due to solidification shrinkage or to entrapped gases. Evidence of localized shear and continuous interparticle melt regions along the shear band was also observed (Figure 4(c)).

In spite of the high hardness of the Ti-Al alloy powders and extensive cracking in these compacts, excellent interparticle bonding was observed. Figures 5(a) through (c) show examples of interparticle melted and resolidified regions in a TiAl compact. The interparticle melt regions solidify to dark etching regions. Figure 5(b) shows an example of localized shear deformation at an inter-

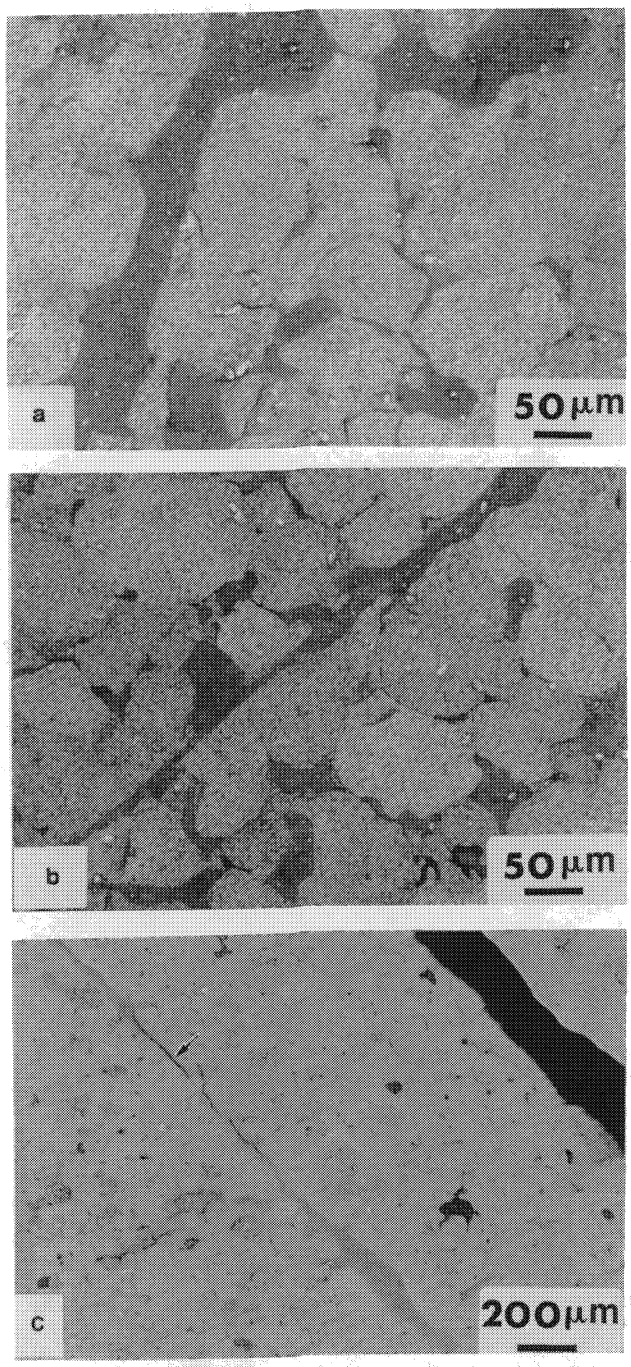

Fig. 5—Optical micrographs showing (*a*) typical interparticle melt regions, (*b*) localized shear deformation and interparticle melting, and (*c*) cracking along shear zone (see arrow).

particle melting region, and Figure 5(c) shows microcracks formed in this region (see arrow).

The additions of Nb powder and mixtures of Ti and Al powders yielded good consolidation with considerable decrease in crack density. In the room-temperature experiments, the addition of Nb resulted in a decrease in cracking for both Ti_3Al and TiAl alloys. Figure 6 shows an optical micrograph in which the Nb particles (white contrast) undergo extensive plastic deformation around the Ti_3Al particles, thereby enhancing the interparticle bonding by providing a binder phase. A similar enhancement and decreased cracking are obtained with TiAl alloy powders mechanically blended with Nb.

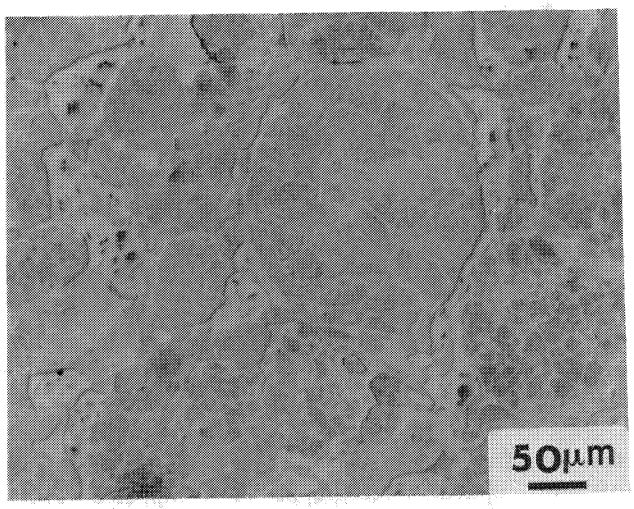

Fig. 6—Optical micrograph of compacted powder showing Nb particles deformed around Ti_3Al particle.

X-ray diffraction results obtained on original as-received Ti_3Al + Nb powder and a typical compact are shown in Figure 7. Some orthorhombic peaks, possibly due to a martensitic transformation, are observed in the compacts. However, the retention of the metastable bcc structure is confirmed, revealing that there are no major structural differences in the original RSP powder and that consolidated by explosive shock waves.

The high-temperature experiments were conducted by preheating the samples at temperatures between 600 °C and 900 °C. Figure 8(a) shows the microstructure of the compacted material, in which niobium particles are plastically deformed around TiAl particles and thus provide

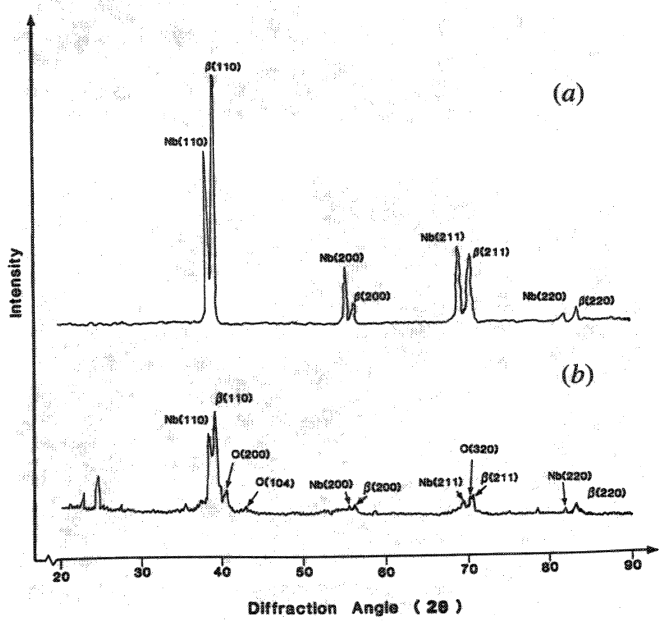

Fig. 7—X-ray diffraction pattern of Ti_3Al + Nb particle powder: (*a*) original as-received powder and (*b*) after compaction (O = orthorhombic).

strong bonding. Figure 8(b) shows the microstructure of the Ti_3Al powder compacted at 600 °C. Gray regions (identified by arrows) indicate the presence of melting and rapid solidification reaction in the interparticle region in both micrographs. Good interparticle bonding is obtained in compacts of preheated powders, as is indicated by transgranular cracking. However, the phase transformation, occurring within Ti_3Al alloy powders after exposure at high temperatures, often causes profuse cracking.

The concept of shock-induced chemical reaction to assist in consolidation was successfully applied to both TiAl and Ti_3Al alloy powders. Approximately 15 wt pct of each Ti and Al elemental powder were mechanically blended to either the Ti_3Al or TiAl powder mixture and shock consolidated at room temperature. Figures 9(a) and (b) show optical micrographs of compacted Ti_3Al and TiAl, respectively. Evidence of chemical reaction between Ti and Al additives was obtained by SEM and EDX analysis. The gray regions in SEM image in Figure 9(c) (indicated by arrows) are reaction products which surround the inert Ti_3Al powders and assist in providing excellent bonding. Unreacted Ti and Al regions are also present in certain locations. This approach resulted in the lowest crack density of all experiments performed.

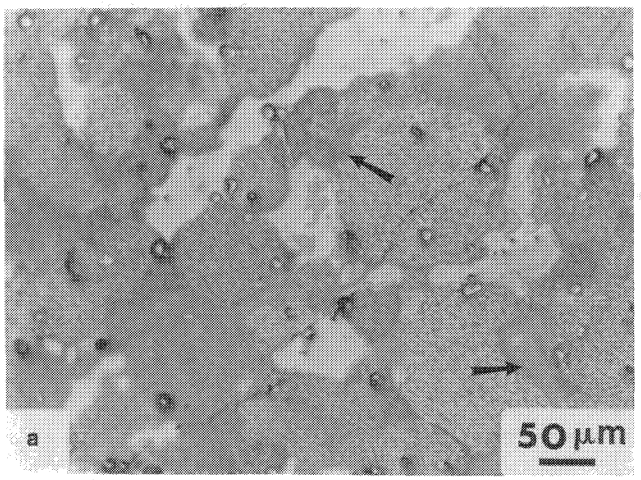

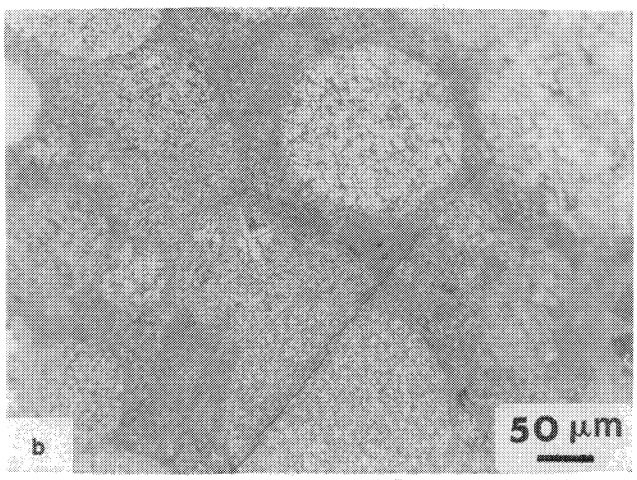

Fig. 8—Optical micrographs of compacted powder from high-temperature experiments (600 °C): (*a*) TiAl + Nb and (*b*) Ti_3Al.

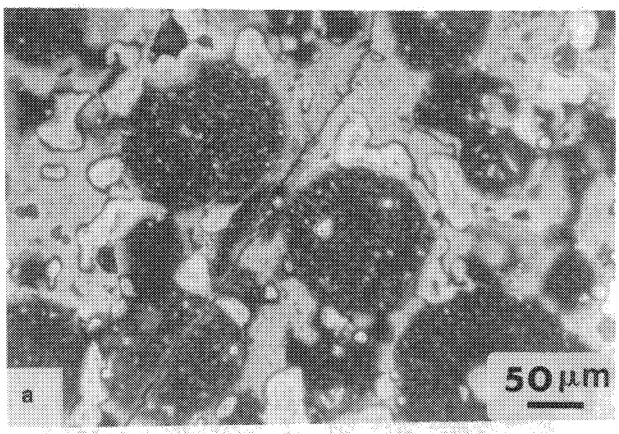

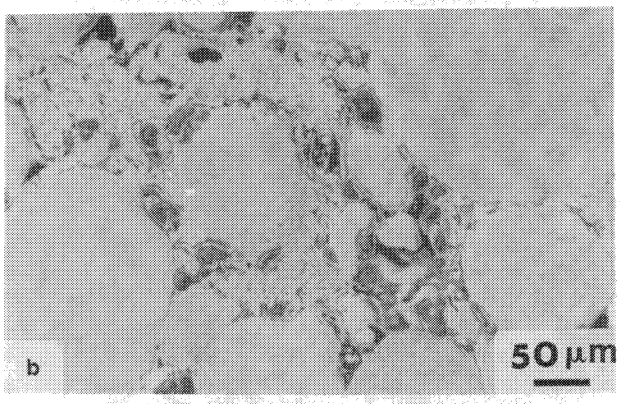

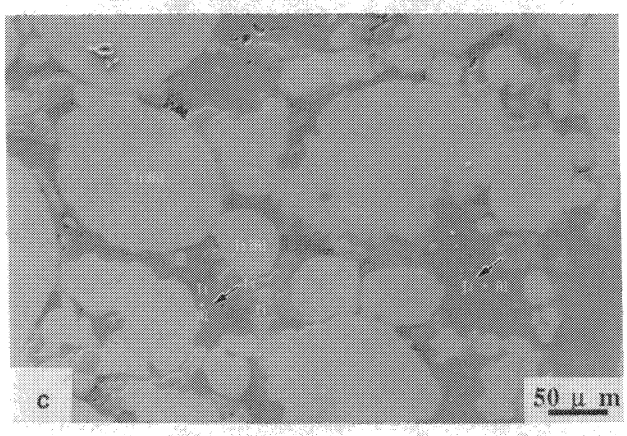

Fig. 9—Optical micrographs of compacts from shock-induced chemical reaction experiments: (*a*) Ti_3Al + Ti + Al and (*b*) TiAl + Ti + Al. (*c*) Scanning electron micrograph from Ti_3Al + Ti + Al in which the different regions were identified by EDX analysis.

C. *Substructure Characterization by TEM Analysis*

Transmission electron microscopy analysis was performed to study the microstructure and substructure of the compacted specimens, in an attempt to determine structural changes in the interparticle regions (due to deformation and localized melting), and within particle interiors (due to shock-induced deformation). Three different titanium aluminide-based alloys (Ti_3Al) compacted at room temperature were observed by TEM: Ti_3Al, Ti_3Al + Nb, and Ti_3Al + Ti + Al powder mixtures.

Figure 10(a) is a bright-field (BF) TEM image from Ti_3Al alloy showing the presence of dislocations and dark round dispersoids. Figure 10(b) is a higher magnification image of these precipitates. Energy-dispersive X-ray analyses confirming the presence of (1) Er_2O_3 precipitates in a (2) Ti_3Al matrix are presented in Figure 10(c). Deformation twinning was also observed as a favored deformation mechanism in some of the Ti_3Al particle interiors. Figure 11 shows a BF and corresponding dark-field (DF) transmission electron micrograph from the same region. Similar deformation substructures (dislocations and deformation twins), typical of shock deformation, have also been observed by Thadhani *et al.*[20] in shock compacted Ni-based superalloys.

Interparticle regions of the shocked compacts showed a different substructure. Figure 12(a) shows a contrast-free interparticle region in the Ti_3Al compact. The contrast-free material is amorphous Ti_3Al, having been produced by melting and rapid resolidification of the interparticle region. The interparticle regions in the compacted Ti_3Al-based alloy mechanically blended with Nb contained both amorphous (light) and crystalline (dark) regions, separated by an irregular interface, as shown in Figure 12(b). The selected area diffraction patterns on the two sides of the interface show the respective structures in the interparticle region. It can also be seen that erbia (Er_2O_3) precipitates are present in the crystalline and amorphous phases, thus giving rise to the crystalline spots in the amorphous pattern. It is interesting to note that the Er_2O_3 precipitates remain unmelted with the otherwise melted and resolidified interparticle regions,

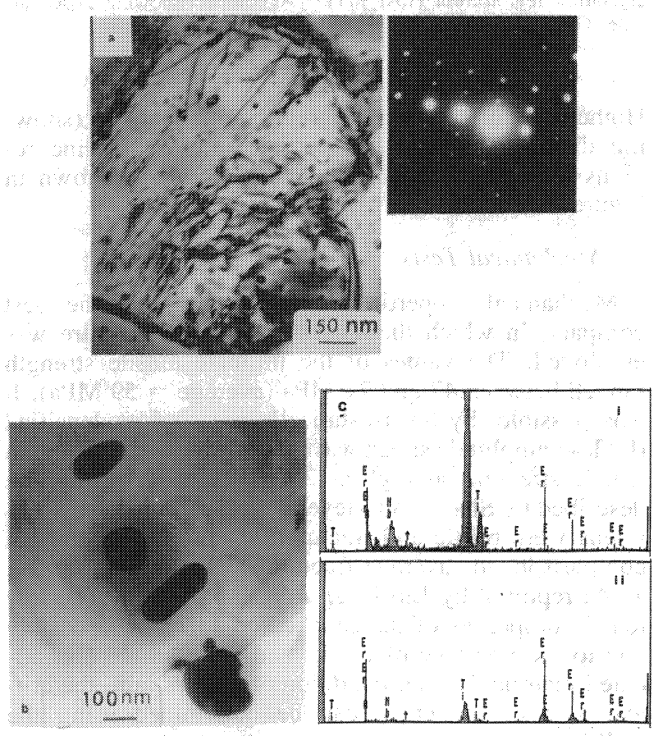

Fig. 10—BF transmission electron micrographs from Ti_3Al-based alloy, compacted at room temperature, showing (*a*) the presence of dislocations in the vicinity of the grain boundary and (*b*) the presence of Er_2O_3 precipitates. (*c*) An EDX of (2) matrix and (1) precipitate.

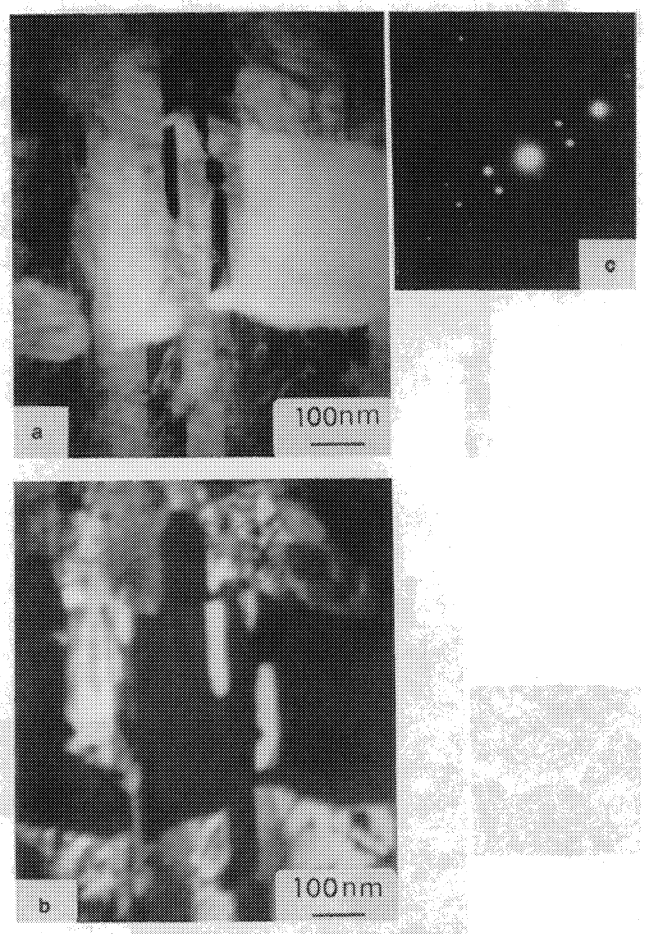

Fig. 11—Deformation twins (or martensite) in Ti_3Al-based alloy compacted at room temperature: (*a*) BF image, (*b*) DF image, and (*c*) twin spots in diffraction pattern.

thus indicating that the interparticle temperature did not exceed 2400 °C (melting temperature of Er_2O_3). The alignment of the Er_2O_3 dispersoids (shown by arrows) in the amorphous phase suggests a solid-state crystalline-amorphous transformation process induced by intense plastic deformation similar to the mechanism proposed by Politis and Johnson,[21] but it would be speculative to comment on this hypothesis at the present stage.

The shock-induced deformation behavior of the Ti_3Al alloy mixed with an elemental mixture of Ti + Al showed different characteristics. More extensive deformation of the particle interiors was observed in contrast to when Ti_3Al powders were consolidated alone. Arrays of dislocations were present within Ti_3Al particle interiors, as shown in Figure 13, which disappeared after tilting the specimen by 6 deg. In some cases, the extensive deformation led to recrystallization of particle interiors. Figures 14(a) and (b) show BF and DF transmission electron micrographs, respectively, of a dislocation-free, 0.5 to 1.0-μm grain size region in a Ti_3Al particle in the Ti_3Al + Ti + Al compact.

The interparticle regions in the Ti_3Al + Ti + Al compact showed presence of a microcrystalline structure. Figure 15(a) is a BF TEM image showing an interface of a Ti_3Al particle (dark) and an interparticle region (light).

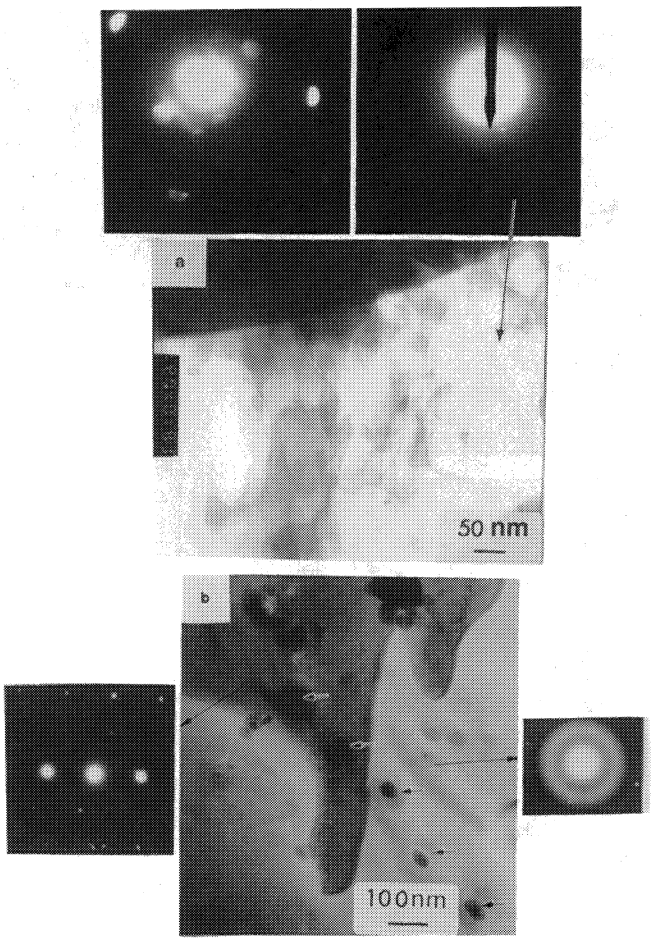

Fig. 12—(*a*) Interparticle amorphous region in shock-consolidated Ti_3Al. (*b*) BF transmission electron micrograph from compacted Ti_3Al-based alloy blended with Nb: amorphous (light) and crystalline (dark) regions, diffraction pattern for amorphous region, and diffraction pattern for crystalline region.

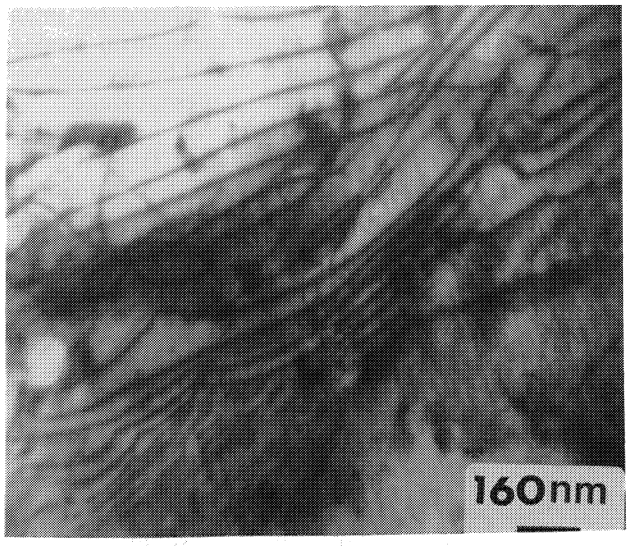

Fig. 13—Transmission electron micrograph from compacted Ti_3Al + Ti + Al alloy showing presence of dislocations.

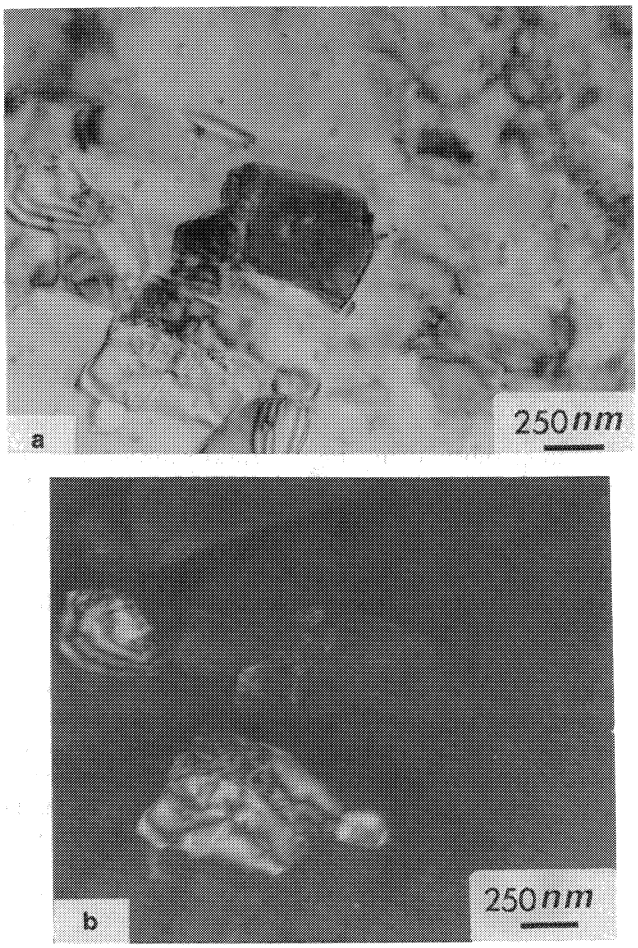

Fig. 14—(*a*) BF and (*b*) DF transmission electron micrographs of crystalline region from Ti_3Al + Ti + Al compact showing Ti_3Al particle. Grain size approximately 0.5 to 1.0 mm.

Higher magnification photographs of the particle (showing dislocations) and interparticle microcrystalline regions (showing 0.2-μm size crystallites) are shown in Figures 15(b) and (c), respectively.

D. *Mechanical Tests*

Mechanical properties were measured on the best compact, in which the Ti_3Al + Ti + Al mixture was employed. The values of the ultimate tensile strength ranged between 47 and 71 MPa (average = 59 MPa). It was possible, by hot isostatically pressing predensified (by low-amplitude shock waves) Ti_3Al powder, to obtain tensile strengths as high as 250 MPa; these results are described by Shang and Meyers.[22] The compacted specimens were brittle and fractured at the elastic limit. In comparison, the average fracture stress for single-phase Ti_3Al reported by Lipsitt *et al.*[3] is 552 MPa. The low tensile properties of the shocked compacts are possibly due to the presence of cracks and voids in the consolidated material. Under condition of plane strain, the critical size of the crack can be determined using the well-known expression:

$$K_{IC} = \sigma_c \pi a_c \left[W \tan \frac{\pi a}{W} \right]^{1/2} \qquad [1]$$

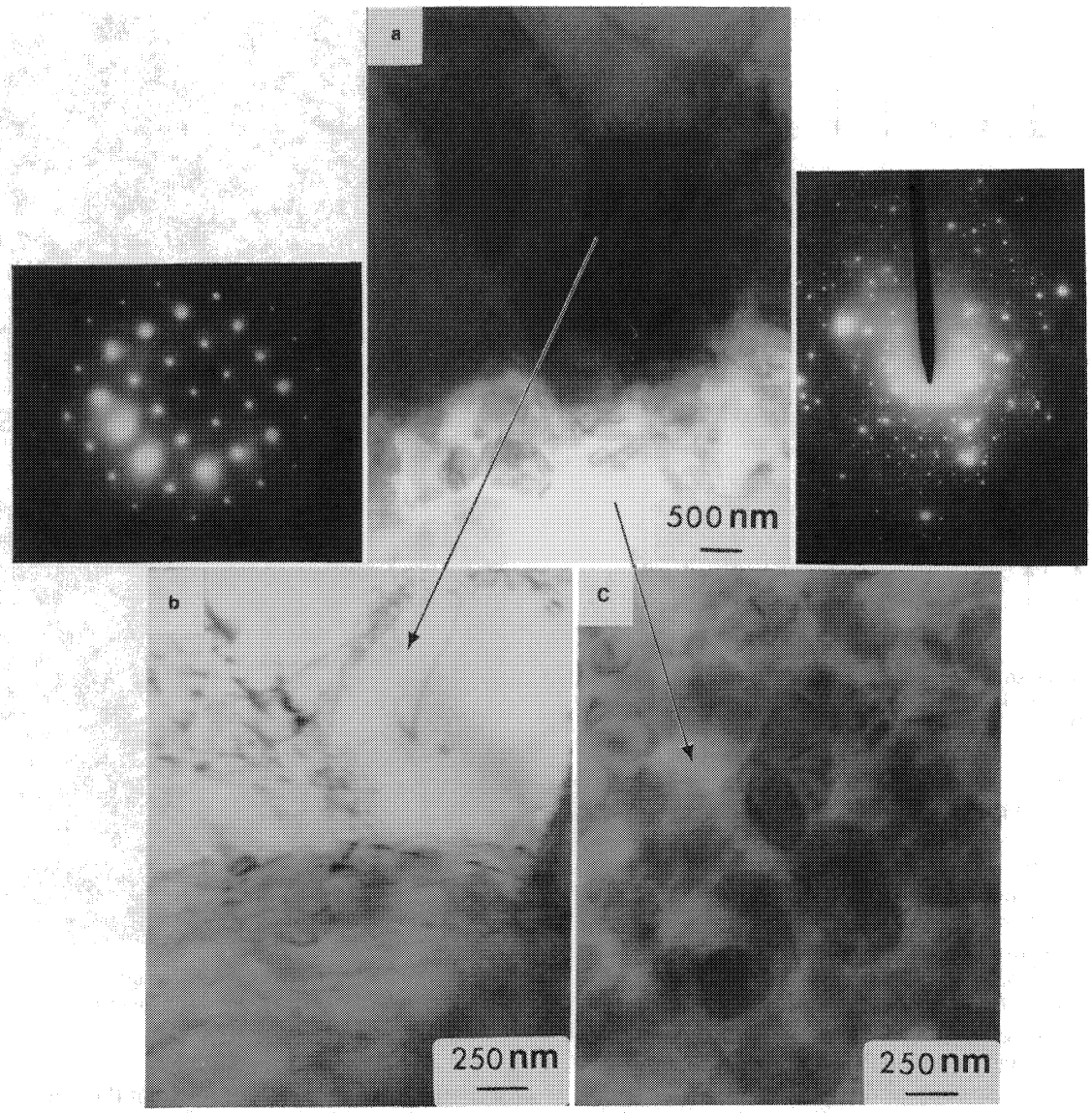

Fig. 15—BF transmission electron micrograph showing (*a*) an interface of Ti_3Al particle in shock-consolidated Ti_3Al + Ti + Al; (*b*) and (*c*) are higher magnification images of the particle and interparticle regions, respectively.

where K_{IC} is the static fracture toughness under conditions of plane strain, σ_c is the critical applied stress acting on the crack, a_c is the critical half crack length, and W is the width of the specimen (4 mm). The value of K_{IC} for Ti_3Al is in the range of 16.5 to 20.0 MPa $m^{1/2}$. By taking an average value of K_{IC} = 18 MPa $m^{1/2}$ and a tensile stress of 59 MPa, one finds that the critical flaw size is equal to 1.9 mm. Interparticle cracks (greater than 2-mm long) were often encountered in the surface of the tensile specimen. Observation of the fracture surface of specimens failed in tension indicates that decohesion may have occurred along the interparticle region due to the presence of pre-existing interparticle cracks and microvoids between particles.

Four compression tests were also carried out on the as-consolidated Ti_3Al + Ti + Al material under identical conditions, and they showed better strength properties when compared with the same material under tensile loading, because the compressive strength is not so sensitive to existing flaws. The ultimate compressive strengths ranged between 1272 and 1731 MPa, with an average of 1456 MPa. The compression specimens failed by a mixture of shear and axial splitting. Axial splitting is produced by tensile stresses developed at the tip of the pre-existing cracks and voids due to the compressive forces. This can be explained by applying the calculations developed by Goodier[23] and inverting the sign of their stresses; these calculations are presented in detail by Timoshenko.[24] By using Goodier's model, spherical voids under compression can give rise to tensile stresses, as shown in Figure 16. The stresses $\sigma_z(\psi = 0, z = 0)$, σ_r, and σ_θ are given by

$$(\sigma_z)_{\psi=\pi/2} = \left[1 + \frac{4 - 5\nu}{2(7 - 5\nu)}\frac{a^3}{r^3} + \frac{9}{2(7 - 5\nu)}\frac{a^5}{r^5}\right]\sigma \quad [2]$$

$$(\sigma_r)_{\psi=0} = (\sigma_\Theta)_{\psi=0} = \left[-\frac{3 + 15\nu}{2(7 - 5\nu)}\right]\sigma \quad [3]$$

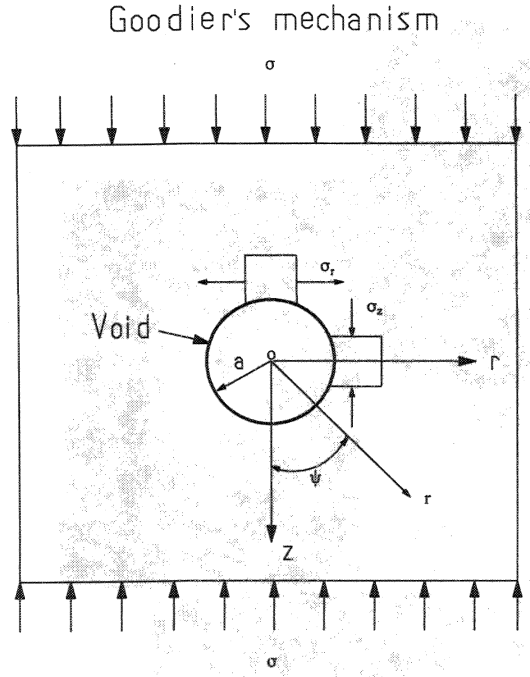

Fig. 16—Stress distribution around a small spherical cavity submitted a uniform uniaxial compression of magnitude s (adapted from Reference 23).

where σ is the applied stress, a is the radius of the void, and ν is the Poisson's ratio of the material.

The stress σ_z decays rapidly with r, as shown in Eq. [2]. An applied compressive stress generates a tensile stress at $\psi = 0$, as shown in Eq. [3]. By using Eq. [3] and assuming $\nu = 0.3$, one arrives at $(\sigma_\theta)_{\psi=0} = -0.682\sigma$. The localized tensile stress is 68.2 pct of the applied compressive stress. Thus, uniaxial compression generates a tensile stress of 670 MPa at an applied compressive stress level of 983 MPa (yield stress in compression). This value is consistent with the value obtained by Lipsitt *et al.*[3] for the tensile strength of Ti_3Al (552 MPa). One can conclude from this that failure in compression is initiated by tensile cracks forming at preexisting voids and flaws. Scanning electron micrographs from the fractured surface reveal a characteristic of brittle fracture (Figure 17). At low magnification and close to the edge (Figure 17(a)), the fracture surface exhibits cleavage regions (indicated by the letter C). Interparticle and transparticle cracks, (indicated by the letters I and T, respectively) are also observed; the latter do not propagate completely through the particle. The interparticle cracks follow a path along the boundaries and might have been caused by differences between the properties of the particle (Ti_3Al) and the reacted regions (Ti + Al) among the particles. At a higher magnification, at the midpoint of the fracture surface (Figure 17(b)), one can see a microvoid (shown by arrow), indicating that the failure may have been initiated at such microvoids.

In the four-point bending test, the maximum flexural stress ranged from 176 to 322 MPa (average = 227 MPa) and maximum shear stress ranged from 26 to 48 MPa (average = 34 MPa). Some voids and microvoids were detected on the surface of the specimen, and they are probable sites for failure initiation. Examination

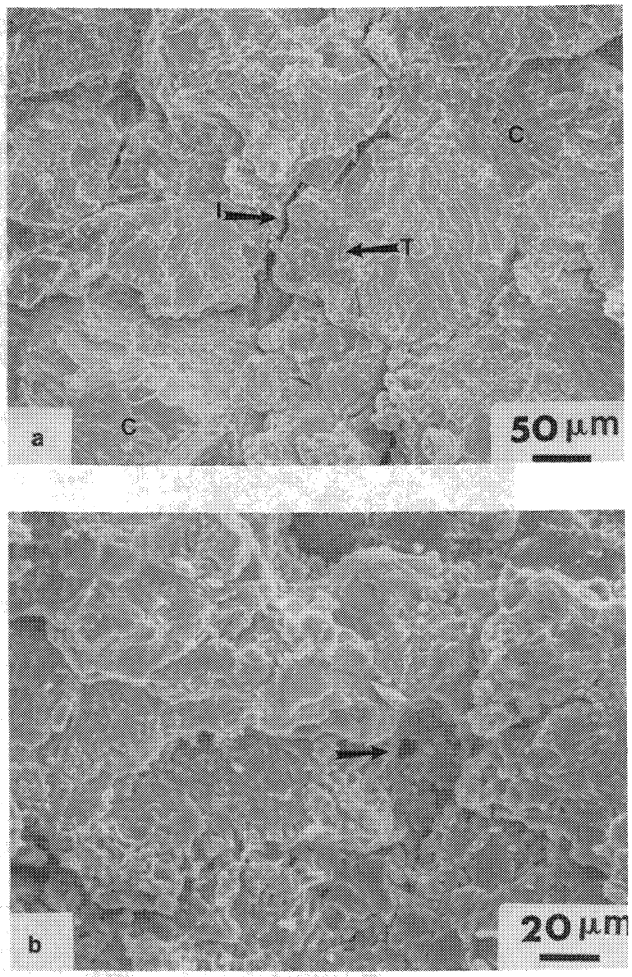

Fig. 17—Fractographs from fractured surface of the specimens in compressive test: (*a*) close to the edge, and (*b*) midpoint of the fracture surface.

of the fracture surface revealed that the failed sample has a faceted aspect, characteristic of the cleavage mode of fracture, which is controlled by tensile stress acting normal to a crystallographic cleavage plane.

IV. CONCLUSIONS

Dynamic compaction of rapidly solidified titanium aluminide powders by explosively generated shock waves is a technique that presents some potential, if cracking can be eliminated. The passage of the shock wave through the powder produced bonding by interparticle melting and resolidification. On a macroscopic level, however, it is difficult to eliminate cracks and flaws that are produced principally by reflected tensile waves. The metastable bcc structure produced by rapid solidification of Ti_3Al was retained in the compacted material. The high-temperature consolidation experiments did not help to produce improved compaction, because the Ti_3Al alloys undergo an embrittling phase transformation upon exposure to temperatures above 500 °C. Additions of Nb and Ti + Al elemental powders helped to provide improved interparticle bonding for both Ti_3Al and TiAl alloy powders.[25] The high cooling rates from the melted region produced fully amorphous regions in which Er-rich

precipitates remained undissolved and unmelted. The Ti_3Al particles exhibited extensive deformation twinning and profuse dislocation arrays as a result of shock-wave passage. A wide range of microstructures was observed in the shock-consolidated materials that depended on the initial microstructure of particles, position within particles (center or interface region), elemental reactions, and heat effects. The mechanical strength obtained in compression is of the same order as that in conventionally processed single-phase Ti_3Al in tension.[3] However, tensile properties (both tensile and four-point bend tests) were poor due to the presence of cracks and microvoids that are developed in the material during the shock consolidation process. A substantial improvement of tensile strength was obtained by hot isostatic pressing ("hipping") shock-densified material.[22] This shock-densified material was subjected to pressures considerably lower (less than one half) the pressures used in the present investigation, thereby minimizing shock-induced cracking. Hipping resulted in the reaction between Ti and Al, thereby providing strong bonding between powders.

ACKNOWLEDGMENTS

This research was sponsored by Pratt & Whitney Government Products Division and by the National Science Foundation Materials Processing Initiative, Award No. DMR 8713258. The partial support of CBMM through the kind help of Dr. J.R.C. Guimaraes is gratefully acknowledged. The authors would like to thank Ms. Sandy Shuleshko (Pratt & Whitney) for her assistance during the work. The help of the CETR Eagle site firing group, Mr. Phil Anthony, Tom Gould, and John LeBarge, who provided assistance in the shock consolidation experiments is greatly appreciated. The use of the facilities of the Center of Excellence for Advanced Materials and of the Electron Optics and Microanalysis Facility is appreciated. Mr. Sun Shang provided valuable help in preparation of specimens for mechanical testing and in the TEM.

REFERENCES

1. Robert E. Schafrik: *Metall. Trans. A*, 1977, vol. 8A, pp. 1003-06.
2. H.A. Lipsitt: *High Temperature Ordered Intermetallic Alloys*, C.C. Koch, C.T. Liu, and N.S. Stoloff, eds., MRS Symp. Proc., Pittsburgh, PA, 1985, vol. 39, p. 351.
3. H.A. Lipsitt, D. Shechtman, and R.E. Schafrik: *Metall. Trans. A*, 1980, vol. 11A, pp. 1369-75.
4. D. Shechtman, M.J. Blackburn, and H.A. Lipsitt: *Metall. Trans.*, 1974, vol. 5, pp. 1373-81.
5. Harry A. Lipsitt, D. Shechtman, and Robert E. Schafrik: *Metall. Trans. A*, 1975, vol. 6A, pp. 1991-96.
6. P.R. Munroe and I. Baker: *Met. Mater.*, 1988, vol. 4, p. 435.
7. P.L. Martin, H.A. Lipsitt, N.T. Nuhfer, and J.C. Williams: *Proc. Conf. on Titanium 80: Science and Technology*, H. Kimura and O. Izumi, eds., TMS-AIME Publication, Warrendale, PA, 1980, p. 1245.
8. S.M.L. Sastry and H.A. Lipsitt: *Metall. Trans. A*, 1977, vol. 8A, pp. 1543-52.
9. D.G. Konitzer and H.L. Fraser: in *High Temperature Ordered Intermetallic Alloys*, C.C. Koch, C.T. Liu, and N.S. Stoloff, eds., MRS Symp. Proc., Pittsburgh, PA, 1985, p. 437.
10. R.G. Rowe, J.A. Sutliff, and E.F. Koch: *Proc. Conf. Rapidly Solidified Alloys and Their Mechanical and Magnetic Properties*, B.C. Giessen, D.R. Polk, and A.I. Taub, eds., MRS Symp. Proc., Pittsburgh, PA, 1986, p. 359.
11. K.R. Teal, A.G. Jackson, D. Eylon, and F.H. Froes: *Proc. Conf. on Titanium: Rapid Solidification Technology*, F.H. Froes and D. Eylon, eds., TMS-AIME Publication, Warrendale, PA, 1986, p. 231.
12. M.A. Meyers and S.L. Wang: *Acta Metall.*, 1988, vol. 36 (4), p. 925.
13. A. Ferreira, M.A. Meyers, N.N. Thadhani, S.N. Chang, and J.R. Kough: *Metall. Trans. A*, 1991, vol. 22A, pp. 685-95.
14. D. Banerjee, A.K. Gogia, T.K. Nandy, and V.A. Joshi: *Acta Metall.*, 1988, vol. 36, p. 871.
15. R. Strychor, J.C. Williams, and W.A. Soffa: *Metall. Trans. A*, 1988, vol. 19, pp. 225-34.
16. M.J. Kaufman, T.F. Broderick, C.H. Ward, J.K. Kim, R.G. Rowe, and F.H. Froes: Washington State University, Seattle, WA, private communication, 1988.
17. M.A. Meyers, B.B. Gupta, and L.E. Murr: *J. Met.*, 1981, vol. 33, p. 21.
18. N.N. Thadhani, A. Mutz, P. Kasiraj, and T. Vreeland, Jr.: in *Metallurgical Applications of Shock-Wave and High-Strain-Rate Phenomena*, L.E. Murr, K.P. Staudhammer, and M.A. Meyers, eds., Marcel Dekker, New York, NY, 1986, p. 247.
19. S.L. Wang, M.A. Meyers, and A. Szecket: *J. Mater. Sci.*, 1988, vol. 23, pp. 1786-96.
20. N.N. Thadhani, A. Mutz, and T. Vreeland, Jr.: *Acta Metall.*, 1989, vol. 37, p. 897.
21. C. Politis and W.L. Johnson: *J. Appl. Phys.*, 1986, vol. 60, p. 1147.
22. Shi-Shyan Shang and Marc A. Meyers: *Metall. Trans. A*, 1991, vol. 22A, pp. 2667-76.
23. J.N. Goodier: *Trans. ASME*, 1933, vol. 55, p. 39.
24. S. Timoshenko: *Theory of Elasticity*, 1st ed., McGraw-Hill, New York, NY, 1934, p. 326.
25. L.H. Yu, M.A. Meyers, and N.N. Thadhani: *J. Mater. Res. Soc.*, 1990, vol. 5, p. 302.